JTTEE5 7:254-260

Plasma Spraying of Combustion Flame Spheroidized Hydroxyapatite (HA) Powders

K.A. Khor, P. Cheang, and Y. Wang

(Submitted 15 January 1997; in revised form 15 April 1997)

Tailoring powder characteristics to suit the plasma spray process can alleviate difficulties associated with the preparation of hydroxyapatite (HA) coatings. Commercial HA feedstock normally exhibit an angular morphology and a wide particle size range that present difficulties in powder transport from the powder hopper to the plasma spray gun and in nonuniform melting of the powders in the plasma flame. Hence, combustion flame spheroidized hydroxyapatite (SHA) was used as the feedstock for plasma spraying. Spherical particles within a narrow particle size range are found to be more effective for the plasma spray processes. Results show coatings generated from spheroidized HA powders have unique surface and microstructure characteristics. Scanning electron microscope (SEM) observation of the coating surface revealed well-formed splats that spread and flatten into disc configurations with no disintegration, reflecting adequate melting of the HA in the plasma and subsequent deposition consistency. The surface topography is generally flat with good overlapping of subsequent spreading droplets. Porosity in the form of macropores is substantially reduced. The cross-section microstructure reveals a dense coating comprised of randomly stacked lamellae. The tensile bond strengths of the SHA coatings, phase composition, and characteristics of the coatings generated with different particle sizes (125 to 75 μm, 45 to 75 μm, 20 to 45 μm, and 5 to 20 μm) showed that a high bond strength of ~16 MPa can be obtained with SHA in the size range from 20 to 45 μm. This can be improved further by a postspray treatment by hot isostatic pressing (HIP). However, larger particle size ranges exhibited higher degrees of crystallinity and relatively higher HA content among the various calcium phosphate phases found in the coatings.

Keywords	bond strength, coatings, hydroxyapatite, phase analysis, plasma spray, powder characterization, XRD

1. Introduction

Coating hydroxyapatite (HA) on bioinert metallic implant surface is an effective method of using this bioactive calcium phosphate compound in the human body (Ref 1, 2). Concerns exist with regard to the wide variation in sintering behavior and resultant mechanical properties of bulk, sintered HA. One drawback on the application of dense, sintered HA is its low fracture toughness, K_{Ic}, and the sensitivity to slow crack growth (Ref 3). This has severely curtailed the use of bulk HA.

Some biological advantages of HA coatings are enhancement of bone formation, accelerated bonding between the implant surface and surrounding tissues, and the reduction of potentially harmful metallic ion release (Ref 4-7). HA has been applied to coat many types of implants such as hip and dental implants (Ref 8, 9). HA also establishes strong interfacial bonds with titanium implants, and this has been attributed to some chemical bonding between HA and the Ti substrate (Ref 10, 11). HA coatings have been applied on various substrates by a wide range of surface deposition techniques such as plasma spraying, high-velocity oxygen fuel (HVOF) spraying, ion beam sputtering, pulsed laser ablation, electrophoretic deposition, radio frequency (rf) magnetron sputtering, sol-gel, and conventional ceramic processes that involve pressing and sintering (Ref 12-20). Among these surfacing processes, thermal spray techniques offer the attractive prospect of economy and efficient deposition of HA. However, HA coatings prepared by plasma spraying have been found to exhibit undesirable phenomena such as formation of amorphous calcium phosphate, tri calcium phosphate (TCP), calcium oxide (CaO), and tetra-calcium phosphate (TTCP) with concomitant reduction of the crystalline HA phase, deviation of the Ca/P stoichiometry, residual stresses, and occurrence of dehydroxylation (Ref 21-26). These detrimental consequences reduce the potency of the HA coatings on the implants.

Adverse effects are able to be reduced significantly through proper process settings and the use of raw material with appropriate characteristics. For instance, plasma spraying of feedstocks with a wide particle size range has resulted in varying crystallinity of the coatings (Ref 27). In addition, the characteristics and properties of the coatings varied when the plasma spray process was performed with different plasma forming gases such as argon (Ar) gas alone, Ar/He, or Ar/H_2. The use of inert gas combinations that are thermally low in enthalpy showed relatively low interfacial strength and poor density, but the HA particles do not undergo significant decomposition. Conversely, the use of Ar/H_2 plasma caused significant decomposition, but it enhanced interfacial strength (Ref 28, 29). One study has indicated contrasting results in the amount of crystalline HA phase and the amount of impurity phases when different plasma forming gases are used (Ref 30). Another study showed that water loss during plasma spraying results in the formation of an OH-depleted hydroxyapatite. At high plasma power, $P_2O_5^-$ ions are lost, and the coatings exhibit more CaO and $Ca_4P_2O_9$

K.A. Khor, Y. Wang, and **P. Cheang,** Nanyang Technological University, Singapore 63 9798, Singapore. Contact e-mail: mkakhor @ntu.edu.sg.

(Ref 31). As a result, the coatings are not able to elicit the desired biological response from surrounding tissues. This setback can be addressed through tailoring the HA powder feedstock to better suit the plasma spray process.

Spherical morphology and narrow particle size range are among the necessary powder characteristics favored in plasma spraying (Ref 32, 33). Spherical morphology will enhance the flowability of the powder feedstock from the powder hopper to the plasma spray gun. Having a narrow particle size range will ensure all the species in the plasma spray remain in the same physical state. The powders should be completely molten, but not superheated in the plasma flame. The molten droplets must not solidify before impacting the substrate surface. The microstructure and properties of plasma sprayed HA coatings are produced with combustion flame spheroidized HA. The spherical geometry of the spheroidized HA has the propensity to provide consistent flow properties that ensure uniform powder feed, and the usage of narrow particle size range will promote uniform melting of the HA in the plasma flame. These in turn provide improved properties on the resultant HA coatings.

2. Experimental Materials and Methods

The raw HA powder was obtained commercially (Kyoritsu Ceramic Materials, Japan) and range from 1 to 150 μm. The particles are angular and contain many small satellites adhering on the surfaces. Table 1 lists the raw HA powder characteristics. Combustion flame spraying was performed with the FP 73 flame torch (Miller Thermal Inc., Wisconsin, MO) using a mixture of oxygen and acetylene gases. The role of combustion flame spray is primarily powder spheroidization. The raw HA powders were flame sprayed into distilled water. A sonic sieve shaker (Fritsch GmbH, Germany) was used to separate the spheroidized powders into the following particle size ranges: 125 to 75 μm, 45 to 75 μm, 20 to 45 μm, and 5 to 20 μm. The flame spheroidized powders, were plasma sprayed on steel plates, Ti-6Al-4V, and stainless steel 316 L stubs to form HA coatings. A 40 kW plasma spray system, the SG-100 (Miller Thermal Inc., Wisconsin, MO), was used to deposit the spheroidized HA feedstock. Argon was the main plasma forming gas, and helium was the auxiliary gas. Powder feed was assisted by a computerized closed loop rotor-feed hopper. Table 2 contains the plasma spray parameters.

Tensile bond strength tests were conducted with an Instron 4302 (10 kN load cell) in accordance to ASTM C 633 at a cross head speed 0.5 mm/min. A hot cured araldite epoxy glue was used as the adhesive. The fracture strength of the adhesive glue is 38.7 MPa. Scanning electron microscopy (SEM) was performed with the Cambridge Stereo Scan S360 (UK) equipped with an energy dispersive x-ray analyzer (EDX) and a wavelength dispersive x-ray (WDX) analyzer.

Phase analysis of the spheroidized HA powders and sprayed HA coatings were performed on the Philips MPD 1880 (Almelo, The Netherlands) x-ray diffractometer (XRD) system using Ni-filtered CuKα radiation at 45 kV and 30 mA. The 2θ range from 20 to 80° was covered at a scan speed of 0.1° min^{-1}. Determination of the crystallinity of the HA was performed by comparing the integrated area intensity of the (211) peak after background subtraction by the profile fit software in the XRD of the as-received HA. The importance of this is that plasma sprayed HA inadvertently contains unspecified amounts of amorphous phases. These obscure the results if only the intensity of the (211) peak was considered since the amorphous phases would also contribute to this value. Thus, the amorphous phase needs to be substrated in the measurement. Accordingly, the crystallinity of the flame spheroidized powder and plasma sprayed coatings is determined.

$$C_r = \frac{A_s}{A_o} \times 100\% \quad \text{(Eq 1)}$$

where C_r is the relative crystallinity of HA, A_o is the integrated area intensity of the as received HA, and A_s is the integrated area intensity of the thermal sprayed (combustion flame or plasma) HA.

3. Results and Discussion

3.1 Microstructure and Phase Analysis of Flame Spheroidized HA Powders and Coatings

Figure 1 shows the SEM view of the flame spheroidized HA. Virtually all the particles below 80 μm have been effectively spheroidized. This confirmed the limit to which the combustion flame spray process has in melting HA, and it agrees well with previous investigations into the melting characteristics of HA in the plasma flame (Ref 34). Particles above this size have rounded edges but not the spherical morphology of well-spheroidized powders.

XRD analysis of the flame spheroidized HA indicates a high crystalline content (Fig. 2). There is relatively little loss in the

Table 1 Chemical analysis and some physical characteristics of as-received HA powders

Chemical composition	CaO 55.36 wt% P_2O_5 41.28 wt%
Calcining temperature	1100 °C, 2h
Ignition loss	2.21%
Average diameter of primary crystallites	2.60 to 5.80 μm
Specific surface area (BET method)	4.41 to 49.9 m^2/g

Table 2 Plasma spray parameters

Primary gas	Argon 82 scfl (50 psi)
Auxiliary gas	Helium 26 scfl (50 psi)
Anode	Forward feed
Cathode	Subsonic
Powder feed rate	20 g/min
Stand off distance	12 to 14 cm

Table 3 Ca/P ratio of flame spheroidized HA powders

Particle size range	Ca/P ratio
5 to 20 μm	1.685
20 to 45 μm	1.698
45 to 75 μm	1.705
75 to 125 μm	1.705
Original HA	1.708

amount in crystalline HA phase in comparison to plasma sprayed HA powders that usually exhibit a presence of tricalcium phosphate (TCP), CaO, and tetra-calcium phosphate (TTCP). However, the relative crystallinity C_r becomes progressively lower with decreasing particle size, and it is consistent with the formation of amorphous calcium phosphate phases when the powders are rapidly quenched (Fig. 3). The smaller particle size ranges would likely be completely molten at the point of impact on the distilled water compared with particles >75 μm where, perhaps, the outer surface may be completely molten, but the inner core of the particles may not have melted. EDX and wavelength dispersive x-ray (WDX) analyses showed a slight variation among the particle size ranges. The small particles showed a lower Ca/P ratio than the large particles (Table 3).

The crystallinity of the particles in the lower particle size ranges can be increased through further heat treatment at 600 to 800 °C prior to plasma spraying. Figure 4 shows the progressive increase in C_r with respect to the heat treatment temperature employed. A significant increase in C_r was observed from 600 to 700 °C.

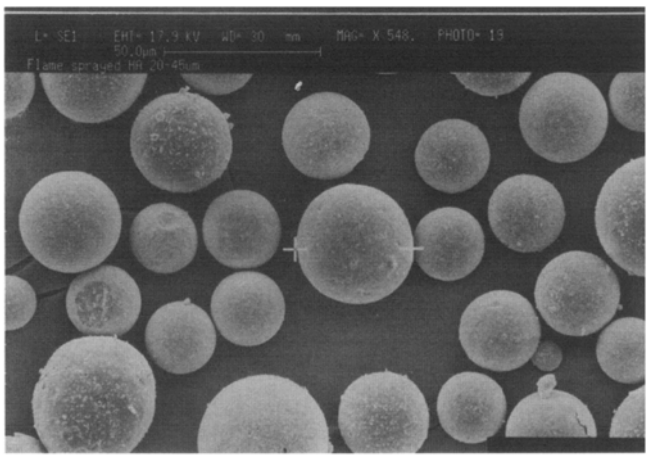

Fig. 1 Scanning electron microscope (SEM) observation of flame spheroidized HA powders. Art reduced 67 percent by printer.

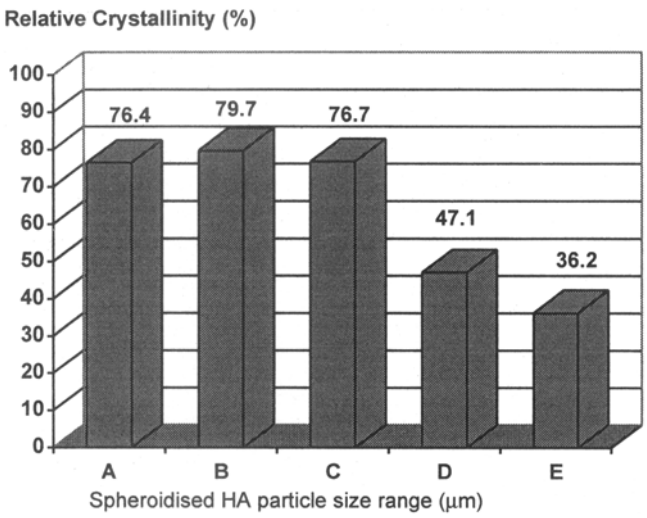

Fig. 3 Relative crystallinity (C_r) of flame spheroidized HA powders with respect to different size ranges (A = all sizes, B = 75 to 125 μm, C = 45 to 75 μm, D = 20 to 45 μm, and E = 5 to 20 μm)

3.2 *Microstructure and Phase Analysis of Plasma Sprayed SHA Coatings*

Coatings generated from spheroidized powders have unique surface and microstructure characteristics. SEM micrographs of the coating surface reveal well-formed splats that spread and flatten into disc configuration without disintegration (Fig. 5). The 75 to 125 μm SHA coating, however, showed evidence of unmelted particles on the surface (Fig. 5b). Good interfacial contact is evident by the absence of visible interlamella pores. Lamella orientation is closely parallel to the substrate, generating a thoroughly uniform coating with good structural integrity. The quality of the spheroidized HA coatings is considerably better than coatings deposited using agglomerated calcined HA and spray dried HA powders. This reflects adequate melting of the HA in the plasma and deposition consistency.

The surface topography is generally flat with good overlapping of subsequent spreading droplets. Porosity in the form of macropores, surrounding unmelted particles, is substantially

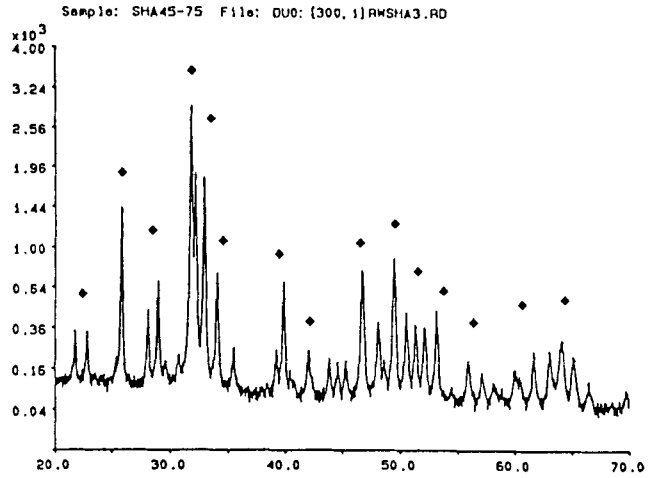

Fig. 2 XRD of flame spheroidized HA powders (45 to 75 μm) ◆ indicates HA

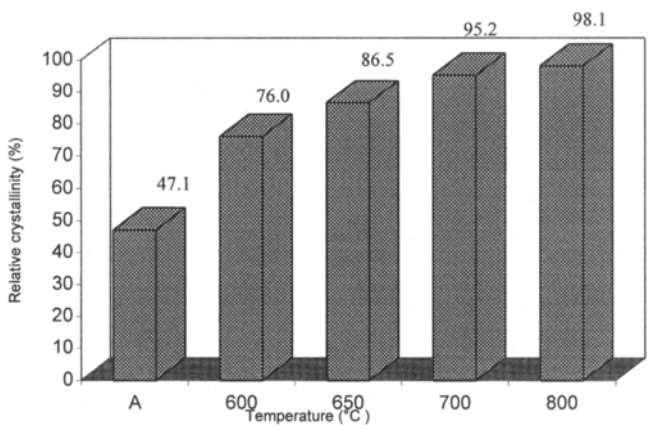

Fig. 4 Progressive increase in C_r of flame spheroidized HA powders following heat treatment. Note: A = as-sprayed coating

reduced and can be further improved using a more accurate control of the plasma energy input during the spraying process. This is evident from the as-sprayed coating structure of SHA (20 to 45 μm, pure HA). Some microcracks are noticeable in coatings >500 μm thick. These cracks are attributed to expansion stressing of the dense matrix. The cross-section microstructure reveals a dense coating comprising of randomly stacked lamellae (Fig. 6a and b). The coating produced with 75 to 125 μm powders, however, contains more pores than the 20 to 45 μm SHA coating. This observation highlights the need for tailoring the plasma spraying condition for each specific particle range.

The XRD pattern (Fig. 7) showed the plasma sprayed SHA coatings contained essentially the phases crystalline HA with some TCP, amorphous calcium phosphate, calcium oxide (CaO), and TTCP phases. The amount of CaO and TTCP in the coatings is higher than in the flame spheroidized powders. The coatings generated with particles in the 20 to 45 μm size range have CaO, TTCP, and TCP as major phases. There is the usual decrease in crystalline HA phase that accompanies the formation of amorphous calcium phosphate phases following the rapid quenching of the liquid droplets during plasma spray. The phase composition of the coatings generated with powders in the 45 to 75 μm and 75 to 125 μm size ranges is essentially the same. There is a significant decrease in the proportion of TCP and TTCP to HA in coatings produced by powders in the size ranges from 45 to 75 and 75 to 125 μm (Table 4). In addition, the formation of CaO was less in the 75 to 125 μm coating. Heat treatment in the temperature range 600 to 800 °C results in the apparent conversion of the TCP, TTCP, and amorphous calcium phosphate phases to crystalline HA and a decrease in the CaO/HA ratio. The decrease in the CaO/HA ratio, however, occurred only

Table 4 Relative amount of HA in plasma sprayed coating as a function of starting particle size

Starting powder size range	TCP/HA	TTCP/HA	CaO/HA
20 to 45 μm	0.68	0.61	0.64
45 to 75 μm	0.40	0.29	0.49
75 to 125 μm	0.33	0.27	0.25

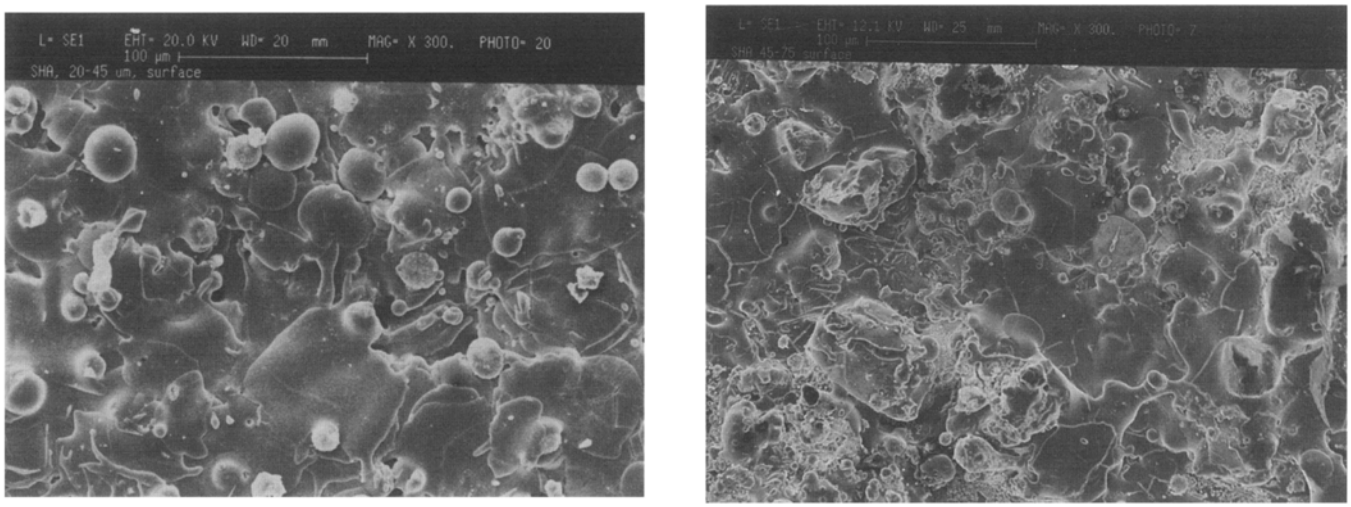

(a) (b)

Fig. 5 SEM view of the as-sprayed coating surface. Art has been reduced 74 percent by printer.

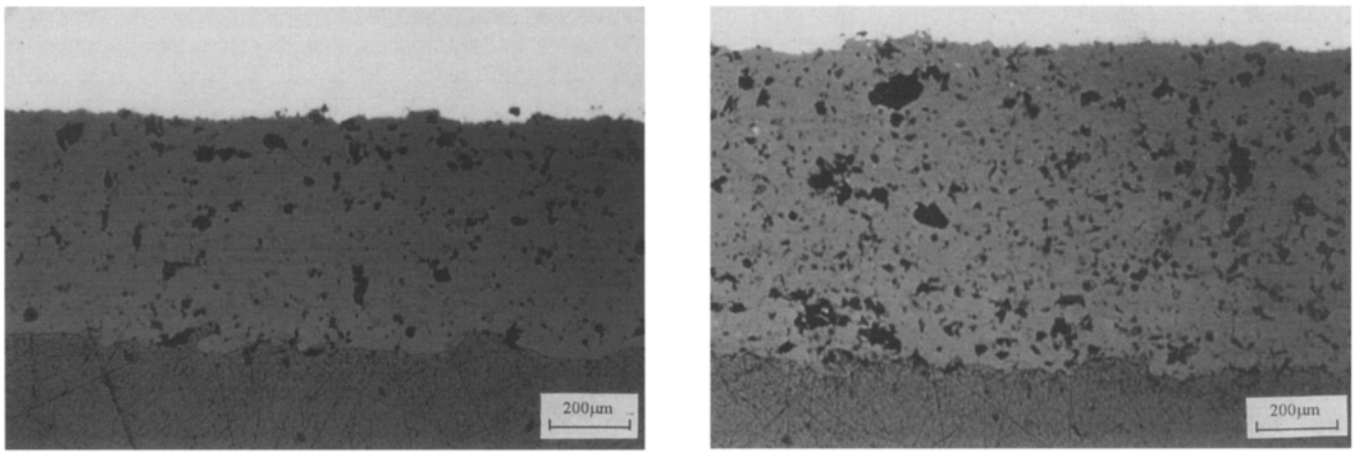

(a) (b)

Fig. 6 Polished cross section of the SHA coating

at 600 °C. Heat treatments at 700 and 800 °C did not result in any further increase in the ratio; rather, there was only a slight increase in the ratio (~6 to 7%). This points to an apparent instability of the calcium phosphates in the coatings above 600 °C.

The long term stability of HA coatings depends on the fractions of the various calcium phosphate phases because of their different levels of solubility in vitro and in vivo (Ref 35, 36). Well crystallized HA coatings show no evidence of resorption in vivo.

The final product formed by plasma spraying is also influenced by the chemical composition of the starting hydroxyapatite powders and plasma spraying conditions. Stoichiometric HA showed least decomposition when plasma sprayed. Table 5 shows the changes in the relative crystallinity (C_r) of the HA phase in plasma sprayed SHA coatings and the relative percentage of HA (X_{HA}) among other crystalline phases, TCP, TTCP, and CaO, in the coatings where:

$$X_{HA} = \frac{I_{HA}}{I_{HA} + I_{TCP} + I_{TTCP} + I_{CaO}} \times 100\% \quad \text{(Eq 2)}$$

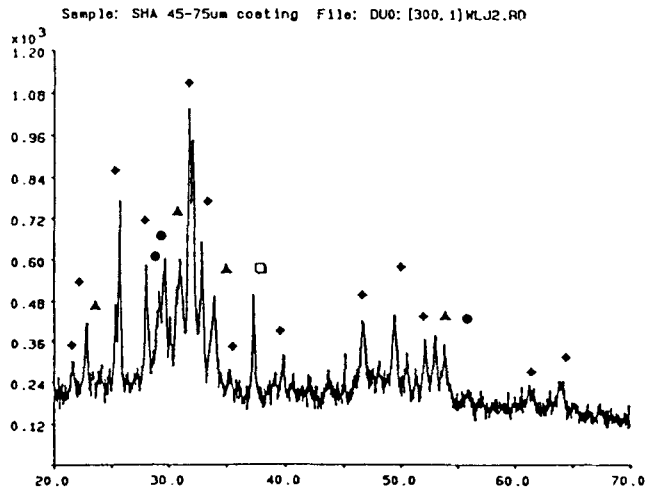

Fig. 7 XRD pattern of SHA coatings (45 to 75 μm powders) ◆ = HA, ▲ = TCP, ● = TTCP, and ❑ = CaO

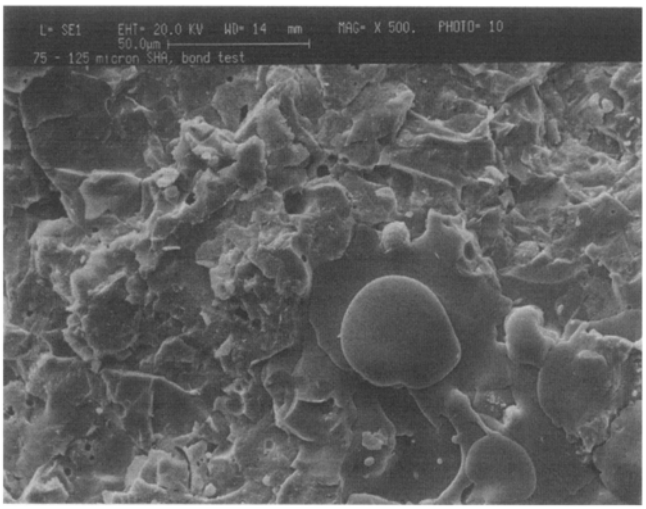

Fig. 8 SEM view of fractured SHA coating

and I_{HA}, I_{TCP}, I_{TTCP}, and I_{CaO} are the integrated area intensities of the HA, α-TCP, TTCP, and CaO peaks, respectively. The coating generated with the smallest particle size range (20 to 45 μm) contained the lowest amount of the crystalline HA phase in both the as-sprayed state and after heat treatment. A correlation appeared between the starting particle size and the C_r value of the coatings with the C_r value increasing with larger starting particles. As expected, the coating produced with 75 to 125 μm powders contained the highest relative crystallinity (C_r) of ~76% after heat treatment at 800 °C. It was also noted that the percentage of crystalline HA phase among the crystalline phases (essentially the HA to CaO ratio) in the coating dipped after 600 °C. Therefore, heat treatment at 700 and 800 °C could result in decomposition of certain unstable calcium phosphate phases to predominantly CaO. This is consistent with observations by McPherson et al. (Ref 31) regarding the loss of P_2O_5 during plasma spraying. The results in Table 5, nevertheless, show a trade-off effect that heat treatment presents, namely, the C_r value in the coating being inversely proportional to the percentage of HA in the coating. The amount of HA among the crystalline phases in the coating is highest after heat treatment at 600 °C, but its C_r value is low (maximum of ~55%). Conversely, the highest C_r value is obtained after heat treatment at 800 °C, and so is the CaO in the coating (hence proportion of HA in the coating is reduced).

The role of CaO in enhancing osseo-induction is not clearly confirmed; however, it is accepted that this phase is biocompatible and mildly bioresorbable. Hence, based on the results of the present study, it would appear that if percentage of HA in the coating plays a major role in the successful application of the implant then a SHA coating produced with 45 to 75 μm or 75 to 125 μm powders and heat treated at 600 °C (or even 700 °C) would be recommended. However, if the C_r value is the determining factor, then the SHA coating produced with the 75 to 125 μm powders would be more appropriate.

The increase in the amounts of amorphous calcium phosphate phase in the plasma sprayed HA coating has been attributed to the loss of hydroxyl groups from the crystalline HA during plasma spraying. The amount of crystalline HA increased when the coatings are subjected to post-spray heat treatment at 600 °C, 700 °C, and 800 °C for 1h. This is consistent with previous observations on plasma sprayed coatings produced with other types of HA starting powders. A recent study on the amorphization phenomena in plasma sprayed HA coatings suggests, based on XRD and infrared spectrometry, that the

Table 5 Changes in C_r and the relative percentage of HA among other crystalline phases TCP, TTCP, and CaO in plasma sprayed SHA coatings in as-sprayed state and after heat treatment

Starting powder size range	Relative crystallinity, C_r, and percentage of HA phase among other crystalline phases (shown in parentheses)			
	As-sprayed	600 °C	700 °C	800 °C
20 to 45 μm	9.4% (34.2%)	50.7% (84.5%)	60.6% (79.7%)	67.1% (75.2%)
45 to 75 μm	18.9% (45.8%)	48.5% (85.5%)	55.5% (81.6%)	71.4% (79.8%)
75 to 125 μm	25.8% (54.0%)	54.8% (92.5%)	61.0% (87.4%)	76.4% (68.5%)

vacancies located on missing hydroxyl sites retard the amorphous/crystalline conversion and enforced retention of the amorphous component (Ref 37). The more vacancies there are in the hydroxyapatite structure due to missing hydroxyl sites, the more amorphous the component in the resultant coatings.

3.3 Mechanical Strength of SHA Coatings

The tensile bond strength of the SHA coatings is relatively higher than HA coatings produced with agglomerated, spray dried HA. Table 6 summarized the adhesive tensile bond strength of the SHA coatings deposited with the various flame spheroidized HA powders on stainless steel and Ti-6Al-4V stubs. SEM observation of the fractured surfaces (Fig. 8) showed failure of the SHA coating as delaminations with some evidence of intra-lamellae cracking.

The high adhesive bond strength of the 60 to 80 μm coatings produced with spheroidized powders in the 20 to 45 μm range indicated that the adhesive bond strength of the HA coatings is influenced by the size of the starting powder. There is an advantage of having small particle size that remained molten up to the point of impact on the substrate surface. Also, the increased amounts of glassy phase in this powder size range ensured better bonding with the Ti substrate surface. The results also indicated the dependence of the adhesive strength on the overall coating thickness where the strength dropped significantly when the coating thickness was increased to ~130 μm. Subsequent post-spray treatment with the hot isostatic press (HIP) showed that the bond strength can be further enhanced, especially for the coatings produced with the 45 to 75 μm and 75 to 125 μm powders.

Table 6 Tensile adhesion properties of SHA coatings

Starting particle size range, μm	Coating thickness, μm	Specific bond strength, MPa		Region of failure
		SS	Ti	
20 to 45	60 to 80		16.6	E/PC
	130		7.1	E/PC
			18.7(a)	E
	>200	6.3		C
45 to 75	70		11.8(a)	E/PC
	≤100		6.2	C
	>200	5.8		C
75 to 125	≤100		94.1	C
	130		121.1(a)	E
	>200	32.2		C

Note: SS is stainless steel stub. Ti is titanium (Ti-6Al-4V) stub. E is failure at epoxy/substrate interface. C is failure within coating. PC is partial failure at coating interface. (a) Specimens that have been HIPed.

Table 7 Cohesive strength of SHA coatings

Number	Coating thickness, μm	Tensile stress, MPa
TS1	300	35.94
TS2	310	26.54
TS3	400	34.70
TS4	320	23.62
TS5	280	29.39
TS6	400	25.20
Mean	**335**	**29.23**

Table 7 shows the cohesive strength of the SHA coatings. The tests were performed similar to the tensile adhesion tests except that the samples were peel-off coatings (~400 μm thick) with the epoxy applied on either side of the coatings. The failure of the coatings was entirely cohesive. EDX analysis did not detect the presence of epoxy in the dense SHA coating. Considering the coherent nature of the coating and the thickness of the coating reaching 400 μm, the possibility of glue interference is less likely. Although a higher cohesive strength is achieved with denser coating, it is only beneficial if the adhesive strength is comparable.

4. Conclusions

The flame spheroidized HA powders can be used as feedstock for plasma spraying of bioceramic coatings. The spheroidized powders above 45 μm predominantly retained the bioactive crystalline HA phase. However, much of the crystalline HA phase was lost upon plasma spraying. Subsequent post-spray heat treatment at 600, 700, and 800 °C for 1 h restored most of the crystalline HA in the coatings. There is a corresponding increase in the crystalline HA phase with starting particle size range. While heat treatment increased the C_T values of the coatings, there is a slight decrease in the HA/CaO ratio at higher temperatures, indicating some instabilities among the calcium phosphate phases at temperatures of 700 and 800 °C.

Tensile adhesion tests indicated the plasma sprayed coatings of the flame spheroidized powders are superior to coatings prepared from the other HA starting powders. Maximum adhesion strength was obtained with particles in the 20 to 45 μm size range, indicating the diverse roles played by the various size ranges. Thus, with appropriate application of the feedstock size, a bioceramic coating with enhanced adhesion, as well as optimum bioactive surface properties, can be achieved. Post-spray HIP treatment enhanced the adhesion bond strength of the coatings. The cohesive strength of the coatings were found to be high (average 29 MPa), thus confirming the excellent inter-lamella bonding in this coating system.

Acknowledgments

Financial support for the plasma spray and HVOF spray systems from NTU RP 56/92 and JT ARC 4/96 is gratefully acknowledged. The hot isostatic press (HIP) unit was financed by a research grant from the Ministry of Finance (Singapore). Technical assistance provided by Mr. Wang Lijun, Mr. Sydney Kwek, and Mdm Yong Mei Yoke is gratefully acknowledged.

References

1. S.D. Cook, K.A. Thomas, J.E. Dalton, T.K. Volkman, T.S. Whitecloud III, and J.F. Kay, Hydroxylapatite Coating of Porous Implants Improves Bone Ingrowth and Interface Attachment Strength, *J. Biomed. Mater. Res.*, Vol 26 (No. 8), 1992, p 989-1001
2. K. de Groot, R. Geesink, C.P.A.T. Klein, and P. Serekian, Plasma Sprayed Coatings of Hydroxyapatite, *J. Biomed. Mater. Res.*, Vol 21 (No. 12), 1988, p 1375-1381
3. G. de With, H. Van Dijk, N. Hattu, and K. Paijs, Preparation, Microstructure, and Mechanical Properties of Dense Polycrystalline Hydroxyapatite, *J. Mater. Sci.*, Vol 16, 1981, p 1592-1598
4. P. Ducheyne, L.L. Hench, A. Kagan, M. Martens, A. Burssens, and J.C. Mulier, The Effect of Hydroxyapatite Impregnation on Skeletal

Bonding of Porous Coated Implants, *J. Biomed. Mater. Res.*, Vol 14, 1980, p 225-237
5. R.G.T. Geesink, K. de Groot, and C.P.A.T. Klein, Bone Bonding to Apatite Coated Implants, *J. Bone Joint Surg.*, Vol 70B, 1988, p 17-22
6. B.C. Wang, E. Chang, D. Tu, and C.Y. Yang, A Histomorphometric Study on Soteoconduction and Osseointegration of Titanium Alloy With and Without Plasma-Sprayed Hydroxyapatite Coating using Back-Scattered Electron Images, *J. Mater. Sci.: Mater. Med.*, Vol 4, 1993, p 394-403
7. P. Ducheyne and K. Healy, Effect of Plasma-Sprayed Calcium Phosphate Ceramic Coatings on the Metal Ion Release from Porous Titanium and Cobalt-Chromium Alloys, *J. Biomed. Mater. Res.*, Vol 22 (No. 12), 1988, p 1137-1163
8. J.A. D'antonio, W.N. Capello, O.D. Crothers, W.L. Jaffe, and M.T. Manley, Early Clinical Experience with Hydroxyapatite-Coated Femoral Implants, *J. Bone Joint Surg.*, Vol 74A (No. 7), 1992, p 995-1008
9. J.F. Kay, Calcium Phosphate Coatings for Dental Implants; Current Status and Future Potential, *Dental Clinics of North America*, Vol 36 (No. 1), 1992, p 1-18
10. R.G.T. Geesink, Hydroxyapatite-Coated Total Hip Prostheses, Two-Year Clinical and Roentgenographic Results of 100 Cases, *Clin. Orthop. Rel. Res.*, Vol 261, 1990, p 39-58
11. H. Ji, C.B. Ponton, and P.M. Marquis, Microstructure Characterization of Hydroxyapatite Coating on Titanium, *J. Mater. Sci.: Mater. Med.*, Vol 3, 1992, p 283-287
12. T.W. Bauer, R.G.T. Geesink, R. Zimmerman, and J.T. McMahon, Hydroxyapatite-Coated Femoral Stems: Histological Analysis of Components Retrieved at Autopsy, *J. Bone Joint Surg.*, Vol 73A (No. 10), Dec 1991, p 1439-1451
13. P. Ducheyne, S. Radin, M. Heughebaert, and J.C. Heughebaert, Calcium Phosphate Ceramic Coatings on Porous Titanium: Effect of Structure and Composition on Electrophoretic Deposition, Vacuum Sintering and in vitro Dissolution, *Biomaterials*, Vol 11, 1990, p 244-254
14. H. Oguchi, K. Ishikawa, S. Ojima, Y. Hirayama, K. Seto, and G. Eguchi, Evaluation of High Velocity Flame Spraying Technique for Hydroxyapatite, *Biomaterials*, Vol 13, 1992, p 471-477
15. W. Van Raemdonck, P. Ducheyne, and D.P. Meester, Auger Electron Spectroscopic Analysis of Hydroxyapatite Coatings on Titanium, *J. Am. Ceram. Soc.*, Vol 67 (No. 6), 1984, p 381-384
16. M. Yoshinari, O. Yoshiro, and T. Dérand, Thin Hydroxyapatite Coating Produced by the Ion Beam Dynamic Mixing Method, *Biomaterials*, Vol 15 (No. 7), 1994, p 529-535
17. J.G.C. Wolke, K. van Dijk, H.G. Schaeken, K. de Groot, and J. Jansen, Study of the Surface Characteristics of Magnetron-Sputter Calcium Phosphate Coatings, *J. Biomed. Mater. Res.*, Vol 28, 1994, p 1477-1484
18. K. Yamashita, T. Arashi, K. Kitagaki, S. Yamada, T. Umegaki, and K. Ogawa, Preparation of Apatite Thin Films Through Rf-Sputtering from Calcium Phosphate Glasses, *J. Am. Ceram. Soc.*, Vol 77 (No. 9), 1994, p 2401-2407
19. C.M. Cotell, D.B. Chrisey, K.S. Grabowski, J.A. Sprague, and C.R. Gossett, Pulsed Laser Deposition of Biocompatible Thin Films: Calcium Hydroxyapatite and Other Calcium Phosphates, *J. Appl. Biomater.*, Vol 3, 1992, p 87-93
20. C. Chai, B. Ben-Nissan, S. Pyke, and L. Evans, Sol-Gel Derived Hydroxylapatite Coatings for Biomedical Applications, *Mater. and Manufacturing Processes*, Vol 10 (No. 2), 1995, p 205-216
21. P.E. Wang and T.K. Chaki, Sintering Behavior and Mechanical Properties of Hydroxyapatite and Dicalcium Phosphate, *J. Mater. Sci.: Mater. Med.*, Vol 4, 1994, p 150-158
22. S.R. Radin and P. Ducheyne, Plasma Spraying Induced Changes of Calcium Phosphate Ceramic Characteristics and the Effect on in vitro Stability, *J. Mater. Sci.: Mater. Med.*, Vol 3, 1992, p 33-42
23. B. Koch, J.G.C. Wolke, and K. deGroot, X-Ray Diffraction Studies on Plasma-Sprayed Calcium Phosphate Coated Implants, *J. Biomed. Mater. Res.*, Vol 24, 1990, p 655-667
24. H.H. Douglas, Overview of Problems Surrounding the Plasma Spraying of Hydroxyapatite Coatings, *Proc. Third NTSC*, Long Beach, CA, USA, ASM International, 1990, p 419-423
25. S.R. Brown, I.G. Turner, and H. Reiter, Residual Stress Measurement in Thermal Sprayed Hydroxyapatite Coatings, *J. Mater. Sci.: Mater. Med.*, Vol 5, 1994, p 756-759
26. M. Weinlaender, J. Beumer, E.B. Kenney, P.K. Moy, and F. Adar, Raman Microprobe Investigation of the Calcium Phosphate Phases of Three Commercially Available Plasma-Flame-Sprayed Hydroxyapatite-Coated Dental Implant, *J. Mater. Sci.: Mater. Med.*, Vol 3, 1992, p 397-401
27. C.P.A.T. Klein, P. Patks, H. van der Lubbe, J.G.C. Wolke, and K. de Groot, Plasma-Sprayed Coatings of Tetracalcium Phosphate, Hydroxylapatite, and Alpha-TCP on Titanium Alloy: An Interface Study, *J. Biomed. Mater. Res.*, Vol 25, 1991, p 53-65
28 W.R. Lacefield, Hydroxyapatite Coating in Bioceramics, P. Ducheyne and J. Lemon, Ed., *Ann. N.Y. Acad. Sci.*, Vol 523, 1988, p 72-80
29. J.G.C. Wolke, J.M.A. De Blieck-Hogervorst, W.J.A. Dhert, C.P.A.T. Klein, and K. de Groot, Studies on the Thermal Spraying of Apatite Bioceramics, *J. Thermal Spray Technol.*, Vol 1 (No. 1), 1992, p 75-82
30. C.Y. Yang, B.C. Wang, E. Chang, and J.D. Wu, Influences of Plasma Spraying Parameters on the Characteristics of Hydroxyapatite Coatings: a Quantitative Study, *J. Mater. Sci.: Mater. Med.*, Vol 6, 1995, p 249-257
31. R. McPherson, N. Gane, and T.J. Bastow, Structural Characterization of Plasma-Sprayed Hydroxylapatite Coatings, *J. Mater. Sci.: Mater. Med.*, Vol 6, 1995, p 327-334
32. D. Bailey, P. Chandler, P. Raymond, and A.R. Nicholl, High Performance Surface Engineering from Plasma Spraying, *Mater. Design*, Vol 9 (No. 6), 1988, p 330-338
33. A.R. Nicholl and H. Eschnauer, Retesting Thermal Spray Powders, *Surf. Coatings Technol.*, Vol 30, 1987, p 95-106
34. K.A.Khor and P. Cheang, Characterization of Thermal Sprayed Hydroxyapatite Powders and Coatings, *J. Thermal Spray Technol.*, Vol 3, 1994, p 45-50
35. P. Ducheyne, S. Radin, and L. King, Effect of Calcium Phosphate Ceramic Composition and Structure on in vitro Behavior, I. Dissolution, *J. Biomed. Mater. Res.*, Vol 27, 1993, p 25-34
36. C.P.A.T. Klein, J.G.C. Wolke, J.M.A. de Blieck-Hogervorst, and K. de Groot, Calcium Phosphate Plasma-Sprayed Coatings and Their Stability: An in vivo Study, *J. Biomed. Mater. Res.*, Vol 28, 1994, p 909-917
37. J. Weng, X. Liu, X. Li, and X. Zhang, Intrinsic Factors of Apatite Influencing Its Amorphization During Plasma-Spray Coating, *Biomaterials*, Vol 16, 1995, p 39-44